

The VAST Survey – I. Companions and the unexpected X-ray detection of B6–A7 stars

R. J. De Rosa^{1*}, J. Bulger¹, J. Patience^{1,2}, B. Leland¹, B. Macintosh², A. Schneider³, I. Song³, C. Marois⁴, J. R. Graham^{5,6}, M. Bessell⁷ & R. Doyon⁸

¹ School of Physics, Exeter University, Stocker Road, Exeter, EX4 4QL, United Kingdom

² Institute of Geophysics and Planetary Physics, Lawrence Livermore National Laboratory, 7000 East Ave, Livermore, CA 94550, USA

³ Physics and Astronomy, University of Georgia, 240 Physics, Athens, GA 30602, USA

⁴ NRC Herzberg Institute of Astrophysics, 5071 West Saanich Road, Victoria, BC, V9E 2E7, Canada

⁵ Astronomy Department, University of California, Berkeley, CA 94720, USA

⁶ Dunlap Institute for Astronomy and Astrophysics, University of Toronto, 50 St. George Street, Toronto, ON, M5S 3H8, Canada

⁷ Mount Stromlo and Siding Spring Observatories, Institute of Advanced Studies, The Australian National University, Weston Creek P.O., ACT 2611, Australia

⁸ Dépt de Physique, Université de Montréal, C.P. 6128, Succ. Centre-Ville, Montréal, QC, H3C 3J7, Canada

15 November 2018

ABSTRACT

With an adaptive optics imaging survey of 148 B6–A7 stars, we have tested the hypothesis that unresolved lower-mass companions are the source of the unexpected X-ray detections of stars in this spectral type range. The sample is composed of 63 stars detected in X-rays within the ROSAT All-Sky Survey and 85 stars that form a control sample; both subsets have the same restricted distribution of spectral type, age, X-ray sensitivity and separation coverage. A total of 68 companion candidates are resolved with separations ranging from $0''.3$ to $26''.2$, with 23 new detections. The multiple star frequency of the X-ray sample based on companions resolved within the ROSAT error ellipse is found to be $43^{+6}_{-6}\%$. The corresponding control sample multiple star frequency is three times lower at $12^{+4}_{-3}\%$ – a difference of $31 \pm 7\%$. These results are presented in the first of a series of papers based on our Volume-limited A-Star (VAST) survey – a comprehensive study of the multiplicity of A-type stars.

Key words: binaries: general – stars: early-type, imaging – X-rays: stars – techniques: high angular resolution

1 INTRODUCTION

The detection of X-ray emission from Main Sequence stars is common (Vaiana et al. 1981), with the notable exception of late B- and early A-type stars (e.g. Stauffer et al. 1994). Two distinct generation mechanisms are responsible for the X-ray emission, related to the different stellar structure of massive O- and B-type stars and lower mass F- to M-type stars. For the massive stars, the hot stellar winds cause X-ray emission, while the lower mass stars produce X-rays from the confinement of superheated plasma within their magnetic fields.

Radiative winds driven by line-absorption and re-emission within the extended atmospheres of O- and early B-type stars form a key component of the model for X-ray emission from these massive stars (e.g. Lucy & White 1980). Wind shocks caused either through instability generated through radiative driving (Owocki et al. 1988), or due to collisions of magnetically driven wind streams (Feldmeier et al. 1997) are thought to be the primary

X-ray generation mechanisms. Interaction between stellar winds and surrounding material is also thought to produce X-rays (e.g. Giampapa et al. 1998).

For lower mass stars, stellar winds are too weak to generate X-rays, and the stellar corona is responsible for the emission of X-rays and is intrinsically linked to the magnetic field. For late A- to early M-type stars, magnetic fields arise from the $\alpha\Omega$ dynamo caused by the differential rotation at the interface between the convective envelope and the radiative core (Spiegel & Weiss 1980). The magnetic field generated by the dynamo process is essential for confining the superheated plasma necessary for X-ray generation (Güdel 2004). The heating mechanism required to maintain the corona at temperatures greater than 10^6 K was originally thought to be acoustic waves (e.g. Schwarzschild 1948; Schatzman 1949), while current models involve Alfvén waves travelling perpendicular to the magnetic field (e.g. De-Pontieu et al. 2007; Jess et al. 2009). Localised magnetic reconnection events within the chromosphere are also a potential source of coronal heating through Joule heating (e.g. Sturrock 1999). Beginning at a spectral type of M3 ($\sim 0.35M_{\odot}$), the stars become fully convective

* E-mail: derosa@astro.ex.ac.uk

(Chabrier & Baraffe 1997) and the high level of magnetic activity observed (e.g. Randich 2000) may be due to an α^2 -type dynamo generation mechanism (Chabrier & Küker 2006), in which turbulent motions are able to generate large-scale magnetic fields.

In addition to the emission mechanisms intrinsic to the star, X-rays can be generated by processes involving binary systems. Accretion of material within cataclysmic variable systems (e.g. Patterson & Raymond 1985) and compact object binaries (e.g. Shapiro et al. 1976) can produce X-ray fluxes. For stars between spectral types B6 to A7, which are expected to be X-ray quiet, the presence of a low-mass companion can lead to the detection of X-rays which are assigned to the primary if the companion is unknown. This study is designed to explore the hypothesis that unresolved lower mass companions are the true source of the unexpected X-ray detections from B6-A7 stars.

2 PREVIOUS OBSERVATIONS

2.1 X-ray detection of B6-A7 stars

Early studies of stellar X-ray emission conducted with the *Einstein Observatory* measured a notable decrease in the fraction of X-ray detected A-type stars ($0.00 \lesssim B - V \lesssim 0.25$) compared to bluer and redder stars (Topka et al. 1982; Schmitt et al. 1985). Out of the 35 A-type stars observed by Schmitt et al. (1985), only 7 were detected and 4 were listed as having a secondary component which could be the source of the X-ray emission. *Einstein* observations of coeval stellar groups also showed a similar decrease in the fraction of X-ray detections of A-type stars between $0.00 \lesssim B - V \lesssim 0.3$ (e.g. Micela et al. 1985; Schmitt et al. 1990).

The increased sensitivity provided by the *ROSAT* mission and all-sky coverage led to the detection and characterisation of a significant number stellar X-ray sources (Voges et al. 1999). A search by Huensch et al. (1998b) of the Bright Star Catalogue (Hoffleit 1964) and the *ROSAT* Bright Source Catalogue for objects within $90''$ of the same position defined a population of 232 B6-A7 X-ray detected stars. To investigate possible sources of the X-ray emission for this sample, the X-ray luminosity was compared with spectral type, spectral peculiarities and rotational velocities (e.g. Simon et al. 1995; Schröder & Schmitt 2007). The lack of a dependence on any of these factors was taken as evidence of unresolved companions. Without a comprehensive binary survey of A-type stars, it was not possible to test the companion hypothesis directly. Similarly, X-ray data from *Chandra* which could resolve the emission source in tight ($\rho \sim 0''.5$) binary systems does not exist for a significant sample of X-ray B6-A7 stars.

2.2 High-resolution imaging companion searches

High resolution AO imaging studies of X-ray detected B- and A-type stars have been employed to search for lower mass stars capable of producing X-rays. Pointed observations of late B-type stars with known lower mass companions (e.g. Schmitt et al. 1993; Berghofer & Schmitt 1994) wide enough to be resolved with the *ROSAT* High Resolution Imager were obtained to determine the source of the X-ray emission. These observations typically identified the B-type star as the source of X-ray emission, although subsequent high-resolution AO imaging has revealed additional components to several of these systems (e.g. Shatsky & Tokovinin 2002). Sub-arcsecond binary companions have also been resolved

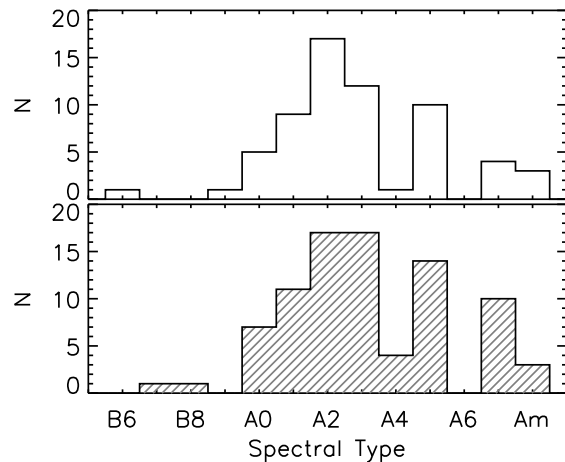


Figure 1. Distribution of the spectral type for each target reported within the *Hipparcos* catalogue for the X-ray (white histogram) and control (grey histogram) samples.

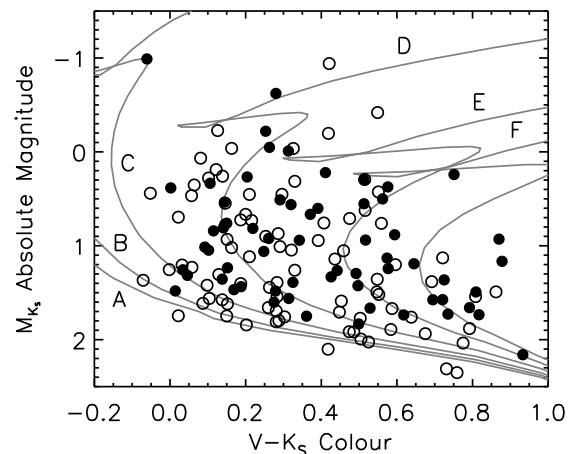


Figure 2. A colour-magnitude diagram of the X-ray (filled circles) and control (open circles) samples. Theoretical isochrones are plotted for A - 10Myrs, B - 100 Myrs, C - 250 Myrs, D - 500 Myrs, E - 800 Myrs, F - 1 Gyrs (Marigo et al. 2008).

with high-resolution AO imaging of pre-Main Sequence companions to late B-type stars (e.g. Hubrig et al. 2001).

Recent discoveries of low-mass companions to Alcor (Mamajek et al. 2010; Zimmerman et al. 2010) and ζ Virginis (Hinkley et al. 2010) have both noted that the unexplained X-ray emission from the primary can be explained by the lower-mass companion, and demonstrate how X-ray emission from A-type stars could be a useful tool in searching for low-mass companions. The current study expands upon the existing imaging results of X-ray detected B6-A7 stars by observing a large sample of both X-ray stars and a control sample.

Table 1. X-Ray Detected Sample

HIP	Name	Hipparcos Spectral Type	Distance <i>pc</i>	ROSAT Source Designation B - BSC, F - FSC	Offset <i>arcsec</i>	Error Radius <i>arcsec</i>	Observations Tel. Date	Magnitude	Band	Integration <i>sec</i>	2MASS Sources <i>arcmin</i> ⁻²
5310	ψ^2 Psc	A3V	49.4±2.0	B - J010757.4+204424	4.9	14	Gemini 16/10/2008	5.22±0.02	K	200	0.156
9480	48 Cas	A3IV	35.8±0.7	B - J020156.9+705432	7.6	8	CFHT 01/09/2009	4.25±0.27	K	480	0.868
11569	ϵ Cas	A5p	43.4±1.5	B - J022902.9+672407	6.4	8	CFHT 05/02/2010	4.25±0.03	K	330	1.088
13133	RZ Cas	A3V+	62.5±2.4	B - J024854.7+693804	4.3	7	Gemini 14/11/2008	5.47±0.02	K	400	0.767
17608	Merope	B6IVe	110.1±12.6	F - J034620.7+235713	24.5	13	AEOS 04/02/2002	4.14±0.03	I	300	0.207
17664		B9.5V	150.1±22.3	F - J034659.4+243049	23.5	23	AEOS 02/03/2003	6.79±0.01	I	599	0.216
17923		A0V	158.7±36.8	B - J034958.2+235109	13.8	14	AEOS 03/02/2002	6.74±0.01	I	289	0.212
19949		A2Vn	108.2±8.8	F - J041642.9+533649	6.7	16	AEOS 05/02/2002	5.15±0.00	I	300	0.749
20070	b Per	A2V	97.6±8.3	B - J041814.8+501747	3.7	7	AEOS 05/02/2002	4.44±0.03	I	300	0.800
20156		A7V	79.4±5.3	B - J041913.6+500254	3.6	8	AEOS 05/02/2002	5.23±0.01	I	300	0.781
20380		A3V	95.0±6.1	F - J042149.8+563020	16.8	27	AEOS 05/02/2002	5.79±0.00	I	300	0.677
20400	60 Tau	A3m	45.7±2.0	F - J042204.5+140440	14.7	27	AEOS 04/02/2002	5.38±0.03	I	300	0.150
20484	63 Tau	A1m	47.2±1.8	F - J042325.5+164633	8.1	28	AEOS 04/02/2002	5.33±0.03	I	300	0.180
20648	δ^3 Tau	A2IV	45.3±1.6	F - J042528.4+175512	31.8	14	AEOS 04/02/2002	4.24±0.03	I	300	0.189
							CFHT 04/02/2010	4.10±0.03	K	352	0.317
21402	88 Tau	A5m	46.1±1.7	B - J043538.5+100941	11.6	8	AEOS 04/02/2002	4.06±0.02	I	300	0.171
22287	4 Cam	A3m	49.7±2.0	F - J044758.6+564531	14.6	18	AEOS 05/02/2002	5.08±0.03	I	300	0.506
23040	7 Cam	A1V	115.2±10.8	B - J045714.3+534442	34.8	10	AEOS 05/02/2002	4.39±0.03	I	300	0.545
23179	ω Aur	A1V	48.8±2.2	B - J045915.4+375330	5.2	7	Gemini 15/11/2008	4.92±0.03	K	200	1.125
23875	β Eri	A4III	27.2±0.6	F - J050750.5+050455	17.3	10	Gemini 19/12/2009	2.40±0.22	K	200	0.274
24019		A5m	54.7±3.9	F - J050945.2+280209	20	12	AEOS 04/02/2002	5.69±0.01	I	300	0.466
26126	38 Ori	A2V	105.8±8.3	F - J053416.4+034623	23.4	17	AEOS 05/02/2002	5.25±0.03	I	300	0.322
28614	μ Ori	A1Vm	46.5±1.8	F - J060222.9+093854	4.6	9	Gemini 19/12/2009	3.64±0.26	K	200	0.995
29997		A0Vn	53.9±1.9	F - J061849.6+691929	18.7	14	CFHT 01/09/2009	4.67±0.02	K	480	0.310
30060	2 Lyn	A2Vs	45.7±2.0	F - J061938.6+590019	22.4	20	AEOS 05/02/2002	4.40±0.00	I	300	0.243
							CFHT 01/09/2009	4.35±0.02	K	480	0.364
30419	ϵ Mon	A5IV	39.4±1.6	B - J062346.2+043544	9.9	10	CFHT 01/09/2009	3.92±0.04	K	480	1.133
35643		A7s	34.5±0.9	F - J072119.0+451327	20.9	22	AEOS 02/02/2002	5.38±0.01	I	300	0.183
39095		A1V	73.1±4.3	F - J075951.6+182353	7.4	17	AEOS 02/02/2002	4.51±0.02	I	300	0.756
39847	27 Lyn	A2V	66.8±3.1	F - J080828.5+513040	19.3	16	AEOS 02/02/2002	4.71±0.04	I	300	0.126
41564		A5m	85.2±6.8	B - J082828.5+023051	13.9	9	AEOS 03/02/2002	6.06±0.01	I	300	0.235
42313	δ Hya	A1Vnn	54.9±2.7	B - J083740.1+054217	11.2	11	AEOS 04/02/2002	4.12±0.02	I	300	0.166
							AEOS 01/03/2003	4.12±0.02	I	300	0.166
44127	ϵ Uma	A7V	14.6±0.2	B - J085913.0+480227	5.9	11	Palomar 12/04/2008	2.66±0.24	K	71	0.145
							CFHT 05/02/2010	2.66±0.24	K	352	0.145
45688	38 Lyn	A3V	37.4±1.1	B - J091850.2+364814	7.5	8	AEOS 06/02/2002	3.81±0.03	I	300	0.081
							Palomar 12/04/2008	3.42±0.35	K	71	0.124
51200		A2V	66.3±3.1	F - J102728.3+413613	9.7	13	CFHT 04/02/2010	5.53±0.02	K	440	0.104
52913	40 Sex	A2IV	95.9±10.8	F - J104917.1+040123	4.7	14	AEOS 02/03/2003	6.38±0.01	I	300	0.083
57646		A3m	62.7±3.2	F - J114915.1+161430	6.4	12	AEOS 02/03/2003	5.75±0.01	I	300	0.058
							CFHT 05/02/2010	5.35±0.02	K	352	0.091
58001	Pheceda	A0Ve	25.6±0.4	B - J115352.3+534153	25	16	Palomar 11/04/2008	2.49±0.17	H	71	0.090
							CFHT 05/02/2010	2.43±0.29	K	352	0.102
59504		A5m	33.7±0.6	B - J121210.1+773702	7.3	20	AEOS 29/05/2002	4.77±0.00	I	300	0.103
62394	34 Vir	A3V	74.6±5.2	F - J124714.4+115723	12.5	19	AEOS 29/05/2002	5.98±0.00	I	300	0.059
62572	AlIIshe	A7V	93.0±15.1	F - J124909.8+832448	6.7	13	AEOS 29/05/2002	5.26±0.00	I	300	0.126
65198		A2V	65.3±3.4	B - J132141.7+020521	7.2	8	AEOS 02/03/2003	5.64±0.00	I	300	0.075
							CFHT 13/06/2008	5.60±0.05	H	450	0.103
							CFHT 04/02/2010	5.51±0.02	K	440	0.115
65241	64 Vir	A2m	63.7±2.9	B - J132209.8+050918	2.6	10	AEOS 03/03/2003	5.82±0.03	I	319	0.066
							CFHT 14/06/2008	5.67±0.03	H	450	0.094
65477	Alcor	A5V	24.9±0.3	F - J132513.8+545920	3.9	13	Palomar 11/04/2008	3.30±0.23	H	71	0.100
66249	ζ Vir	A3V	22.5 ± 0.4	F - J133442.6+003530	19.6	14	AEOS 03/03/2003	3.27±0.02	I	300	0.079
							CFHT 05/02/2010	3.22±0.27	K	352	0.122
66727	1 Boo	A1V	92.8±7.8	B - J134040.2+195708	12.8	11	AEOS 03/03/2003	5.72±0.01	I	300	0.064
71618	33 Boo	A1V	60.4±2.0	B - J143850.0+442418	3.7	7	CFHT 14/06/2008	5.28±0.04	H	450	0.098
76376		A2V	75.5±3.0	B - J153556.8+54375	3.3	9	AEOS 29/05/2002	5.72±0.00	I	300	0.089
76878	τ^7 Ser	A2m	53.2±2.3	B - J154154.9+182744	6.9	15	AEOS 29/05/2002	5.61±0.03	I	300	0.096
							Palomar 13/07/2008	5.30±0.02	K	62	0.149
77336	ν Ser	A3V	77.2±6.0	F - J154717.7+140652	7.3	16	AEOS 29/05/2002	5.61±0.00	I	300	0.108
80628	ν Oph	A3m	37.5±1.2	B - J162748.2+082213	4.8	9	Palomar 12/04/2008	4.17±0.04	K	47	0.401
82321	52 Her	A2Vspe	53.7±1.5	F - J164914.1+455848	12	12	Palomar 12/07/2008	4.58±0.04	H	71	0.174
83223		A7V	73.1±4.6	F - J170028.6+063456	13.4	29	AEOS 29/05/2002	6.33±0.01	I	300	0.232
85829	ν^2 Dra	A4m	30.6±0.5	F - J173216.1+551023	1	15	Palomar 12/04/2008	4.16±0.02	K	71	0.203
							CFHT 05/02/2010	4.16±0.02	K	264	0.223
87045		A2Vs	131.6±14.2	B - J174707.6+473648	5.2	8	AEOS 29/05/2002	6.37±0.01	I	300	0.183
87212	30 Dra	A2V	66.5±2.1	F - J174904.5+504651	2.6	34	Gemini 24/06/2008	4.88±0.02	K	200	0.259
							Palomar 12/07/2008	4.88±0.02	K	71	0.259
88771	72 Oph	A4IVs	25.4±0.5	F - J180719.8+093411	26.4	16	Palomar 12/04/2008	3.41±0.19	K	71	0.990
							CFHT 05/02/2010	3.41±0.19	K	264	0.990
89925	108 Her	A5m	57.6 ± 2.0	F - J182057.4+295146	14.8	12	AEOS 31/05/2002	5.37±0.03	I	300	0.348
							Gemini 24/06/2008	4.99±0.02	K	200	0.540
							CFHT 01/09/2009	4.99±0.02	K	720	0.540
91971	ζ^1 Lyr	Am	47.1±1.2	B - J184446.1+373620	3.7	9	CFHT 13/06/2008	3.97±0.23	K	180	0.566
93747	ζ Aql	A0Vn	25.5±0.5	B - J190526.0+135136	22.8	12	CFHT 13/06/2008	3.05±0.28	H	180	5.932
98103	ϕ Aql	A1IV	63.1±3.0	F - J195613.8+112526	8.5	13	Gemini 18/06/2008	5.26±0.02	K	200	1.778
102033		A2V	82.0±4.4	F - J204036.8+294822	6.1	15	AEOS 31/05/2002	5.87±0.00	I	300	0.993
106711	74 Cyg	A5V	63.3±2.5	F - J213656.7+402440	8.9	14	Gemini 08/09/2008	4.51±0.02	K	200	1.218
109521		A5V	54.8±1.7	B - J221109.0+504929	8.7	14	Gemini 08/09/2008	4.96±0.02	K	200	2.059
110787	ρ^1 Cep	A2m	62.6±2.0	F - J22264.9+784709	4.5	12	Gemini 17/08/2008	5.54±0.03	K	200	0.435
117452	δ Scl	A0V	44.0±2.2	B - J234854.7-280751	11.2	13	CFHT 30/08/2009	4.53±0.02	K	480	0.112

3 SAMPLE

Two samples were constructed in order to test the companion hypothesis: a 63-star X-ray detected sample, and an 85-star control sample. The distributions of spectral types reported in the *Hipparcos* catalogue for both samples are shown in Figure 1, and a K-S test confirms that both are drawn from the same distribution. The majority of the total sample, 108 targets, form a part of our ongoing Volume-limited A-Star (VAST) survey which will include all A-type stars within 75 parsecs. Both the X-ray and control samples includes targets spanning a similar range of ages, as shown in the

colour-magnitude diagram in Figure 2. To perform a robust test of the companion hypothesis, we ensured that each sample had a similar distribution of sensitivity to X-ray sources. Background X-ray counts were extracted from the *ROSAT* All Sky Survey (RASS) observations at the coordinates of each target within both samples. A minimum detectable X-ray flux at each coordinate was estimated as five times the background level. These minimum fluxes were calculated assuming a hardness ratio of 0.5, typical of low-mass stellar sources (e.g. Huélamo et al. 2000). The X-ray luminosity (L_X) was then calculated based on a distance equal to that of the target.

Table 2. Control Sample

HIP	Name	Hipparcos Spectral Type	Distance <i>pc</i>	Observations Tel.	Date	Magnitude	Band	Integration <i>sec</i>	2MASS Sources <i>arcmin</i> ⁻²
159		A3	59.1±2.8	Gemini	17/10/2008	6.21±0.02	K	200	0.115
2852		A5m	49.7±2.2	Gemini	17/10/2008	5.42±0.02	K	200	0.100
3414	π Cas	A5V	53.5±2.1	AEOS	02/03/2003	4.79±0.01	I	300	0.334
				Gemini	16/10/2008	4.58±0.02	K	200	0.505
5317	41 And	A3m	60.2±2.7	Gemini	16/10/2008	4.77±0.02	K	200	0.404
8122		A3	71.7±3.8	CFHT	30/08/2009	6.17±0.02	K	640	0.229
9487	α Psc	A2	42.6±1.9	CFHT	01/09/2009	3.62±0.33	K	480	0.115
13717		A1Vn	57.9±3.1	Gemini	18/10/2008	4.86±0.02	K	200	0.115
17489	Celero	B7IV	102.6±11.1	AEOS	03/02/2002	5.43±0.03	I	300	0.207
17572		A0V	103.3±11.0	AEOS	04/02/2002	6.77±0.01	I	300	0.192
17588	22 Tau	A0Vn	108.6±10.9	AEOS	02/02/2002	6.41±0.03	I	300	0.213
17791		A1V	144.9±20.8	AEOS	04/02/2002	6.83±0.02	I	300	0.217
17847	Atlas	B8III	116.7±14.0	AEOS	04/02/2002	3.64±0.03	I	300	0.214
20507	ξ Eri	A2V	63.9±3.3	Gemini	17/10/2008	4.93±0.02	K	200	0.187
20641	κ^2 Tau	A7	44.2±1.6	CFHT	05/02/2010	4.61±0.02	K	352	0.362
20894	θ^2 Tau	A7III	45.7±1.7	CFHT	04/02/2010	2.88±0.26	K	440	0.307
21039	81 Tau	Am	44.3±2.1	CFHT	05/02/2010	4.90±0.02	K	352	0.311
22192	EX Eri	A3IV	57.5±2.2	Gemini	14/11/2008	5.72±0.02	K	200	0.172
23554		A2IV	60.1±2.3	Gemini	19/12/2009	5.34±0.02	K	200	0.209
23983	16 Ori	A2m	53.9±2.4	Gemini	05/11/2008	4.86±0.02	K	200	0.403
25197	16 Cam	A0Vne	104.3±8.4	AEOS	05/02/2002	5.23±0.00	I	300	0.337
26309		A2III-IV	56.6±2.3	Gemini	14/11/2008	5.86±0.02	K	200	0.255
28360	Menkalinan	A2IV+	25.2±0.5	CFHT	05/02/2010	1.78±0.19	K	352	0.651
28910	θ Lep	A0V	52.2±1.9	Gemini	25/11/2008	4.52±0.02	K	200	0.472
29711		A5IVs	66.5±3.4	Gemini	25/11/2008	5.86±0.02	K	200	0.729
31119		A3V	64.8±3.6	AEOS	04/02/2002	5.04±0.01	I	300	0.706
				Gemini	11/11/2008	4.77±0.04	K	200	1.198
31290		A3V	136.1±18.0	AEOS	05/02/2002	6.46±0.01	I	300	0.402
34897		A5	66.4±3.4	Gemini	10/05/2010	5.99±0.02	K	200	0.293
35341	65 Aur	A5Vn	82.1±6.2	AEOS	02/02/2002	5.69±0.01	I	300	0.207
35350	λ Gem	A3V	28.9±0.8	Palomar	12/04/2008	3.54±0.26	K	68	0.489
				CFHT	04/02/2010	3.54±0.26	K	440	0.489
38723		A3p	60.4±3.4	Gemini	11/11/2008	5.40±0.02	K	200	0.241
40646	29 Lyn	A7IV	93.2±5.9	AEOS	03/02/2002	5.46±0.00	I	300	0.116
41152		A3V	51.4±1.9	AEOS	06/02/2002	5.39±0.01	I	300	0.113
42806	Asellus Borealis	A1IV	48.6±2.0	AEOS	02/03/2002	4.64±0.00	I	300	0.123
43570		A5V	167.8±38.8	AEOS	04/02/2002	6.21±0.01	I	300	0.138
43932	σ^2 Cnc	A7IV	59.8±3.3	AEOS	06/02/2002	5.26±0.01	I	300	0.099
44066	α Cnc	A5m	53.2±2.8	AEOS	01/03/2003	4.13±0.03	I	300	0.119
44901	15 UMa	A1m	29.3±0.7	AEOS	01/03/2003	4.19±0.03	I	300	0.087
				Palomar	12/04/2008	4.04±0.28	K	69	0.138
				CFHT	05/02/2010	4.04±0.28	K	352	0.138
45493	18 UMa	A5V	36.3±1.0	AEOS	03/03/2003	4.58±0.03	I	300	0.094
				Palomar	12/04/2008	4.29±0.02	K	85	0.138
49593	21 LMi	A7V	28.0±0.7	Palomar	12/04/2008	4.00±0.04	K	44	0.108
51658		A7IV	34.3±0.9	Palomar	12/04/2008	4.20±0.02	K	69	0.106
				CFHT	04/02/2010	4.20±0.02	K	440	0.106
53910	Merak	A1V	24.4±0.4	CFHT	04/02/2010	2.29±0.24	K	440	0.106
53954	60 Leo	A1m	37.9±1.2	Palomar	12/04/2008	4.32±0.04	K	71	0.103
54063		A5	61.8±3.3	CFHT	14/06/2008	6.29±0.02	H	450	0.079
54136	51 UMa	A3III-IV	80.6±4.6	AEOS	03/03/2003	5.86±0.01	I	300	0.065
57328	ξ Vir	A4V	36.6±1.1	AEOS	03/03/2003	4.67±0.00	I	300	0.067
				Palomar	11/04/2008	4.41±0.05	K	71	0.104
				CFHT	13/06/2008	4.54±0.08	H	180	0.091
57632	β Leo	A3V	11.1 ± 0.1	CFHT	05/02/2010	1.88±0.19	K	352	0.099
58510	7 Vir	A1V	84.8±5.4	AEOS	02/03/2003	5.34±0.00	I	290	0.068
58590	π Vir	A5V	109.2±10.1	AEOS	02/03/2003	4.53±0.02	I	300	0.067
59394	3 Crv	A1V	56.1±2.1	CFHT	14/06/2008	5.36±0.04	H	450	0.165
59608	12 Vir	A2m	49.5±1.8	AEOS	03/03/2003	5.61±0.03	I	200	0.060
				CFHT	04/02/2010	5.24±0.02	K	440	0.097
59774	Megrez	A3V	25.0±0.4	Palomar	11/04/2008	3.31±0.25	H	71	0.094
				CFHT	13/06/2008	3.31±0.25	H	180	0.094
60746	16 Com	A4V	86.5±5.6	AEOS	03/02/2003	4.93±0.03	I	300	0.058
61960	ρ Vir	A0V	36.9±1.1	AEOS	02/03/2003	4.80±0.03	I	300	0.064
				Palomar	11/04/2008	4.76±0.02	H	57	0.092
				CFHT	04/02/2010	4.68±0.02	K	440	1.040
62933	41 Vir	A7III	61.0±2.9	CFHT	05/02/2010	5.47±0.02	K	352	0.097
68520	τ Vir	A3V	66.9±3.9	AEOS	03/03/2003	4.11±0.02	I	300	0.075
69592		A7V	59.0±2.6	Palomar	12/07/2008	5.90±0.02	H	71	0.093
69732	λ Boo	A0p	29.8±0.5	AEOS	03/03/2003	4.15±0.03	I	300	0.069
				Palomar	11/04/2008	4.03±0.25	H	71	0.095
69951		A5	73.5±3.4	Palomar	12/07/2008	6.40±0.04	H	71	0.097
69974	λ Vir	A1V	57.2±3.1	AEOS	03/03/2003	4.43±0.02	I	669	0.114
				Gemini	24/06/2008	4.24±0.02	K	200	0.177
71075	γ Boo	A7III	26.1±0.5	Palomar	11/04/2008	2.57±0.25	H	71	0.089
75043		A4V	65.3±2.2	AEOS	29/05/2002	5.52±0.00	I	300	0.082
76852	ι Ser	A1V	58.9±2.7	Palomar	13/07/2008	4.31±0.02	K	71	0.142
77233	β Ser	A3V	46.9±1.9	Palomar	12/04/2008	3.55±0.32	K	67	0.161
77464		A5IV	49.2±1.7	Gemini	27/06/2008	5.26±0.02	K	200	0.238
77622	ϵ Ser	A2m	21.6±0.3	Palomar	12/04/2007	3.43±0.27	K	71	0.203
83613	60 Her	A4IV	44.1±1.4	Palomar	12/04/2008	4.61±0.02	K	71	0.347
84012	η Oph	A2IV-V	25.8±0.6	Palomar	12/04/2008	2.34±0.24	K	71	1.436
86565	\circ Ser	A2Va	51.5±2.8	Gemini	28/06/2008	4.11±0.25	K	200	3.249
87108	γ Oph	A0V	29.0±0.8	Palomar	12/04/2008	3.62±0.23	K	71	0.919
				CFHT	31/08/2009	3.62±0.23	K	480	0.919
92161	111 Her	A5III	28.4±0.6	CFHT	13/06/2008	4.08±0.03	H	180	1.472
95081	π Dra	A2III	68.9±2.2	Gemini	24/06/2008	4.45±0.02	K	200	0.380
				Palomar	12/07/2008	4.58±0.17	H	71	0.348
95853	ι^2 Cyg	A5Vn	37.5±0.6	CFHT	12/06/2008	3.69±0.23	H	280	0.583
99655	33 Cyg	A3IV-Vn	46.7±1.0	CFHT	14/06/2008	4.17±0.27	H	450	0.767
99742	ρ Aql	A2V	47.1±1.7	CFHT	30/08/2009	4.77±0.02	K	480	1.353
99770	29 Cyg	A2V	41.0±0.9	CFHT	31/08/2009	4.42±0.02	K	480	7.030
100108	36 Cyg	A2V	59.7±1.9	AEOS	31/05/2002	5.51±0.00	I	300	2.521
				Gemini	08/09/2009	5.49±0.02	K	200	6.666
100526		A2	69.2±2.2	Gemini	08/09/2008	6.20±0.02	K	200	1.137
101093	θ Cep	A7III	41.6±0.9	CFHT	30/08/2009	3.72±0.32	K	200	0.662
101300		Am	81.1±4.6	AEOS	31/05/2002	6.08±0.01	I	300	0.980
101483	η Del	A3IVs	53.0±2.3	Gemini	08/09/2008	5.24±10.00	K	200	0.796
105966	35 Vul	A1V	55.7±2.2	Gemini	08/09/2008	5.29±0.02	K	200	0.630
109427	θ Peg	A1 Va	29.6±0.8	CFHT	14/06/2008	3.39±0.21	H	450	0.193
109667		A3V	58.1±2.7	Gemini	10/09/2008	5.74±0.02	K	200	0.157
				CFHT	31/08/2009	5.74±0.02	K	720	0.157
111169	α Lac	A1V	31.4±0.5	Palomar	12/07/2008	3.87±0.21	H	71	1.384
				CFHT	30/08/2009	3.85±0.27	K	480	1.516
116354	15 And	A1III	71.6±3.2	Gemini	08/09/2008	5.28±0.02	K	200	0.405

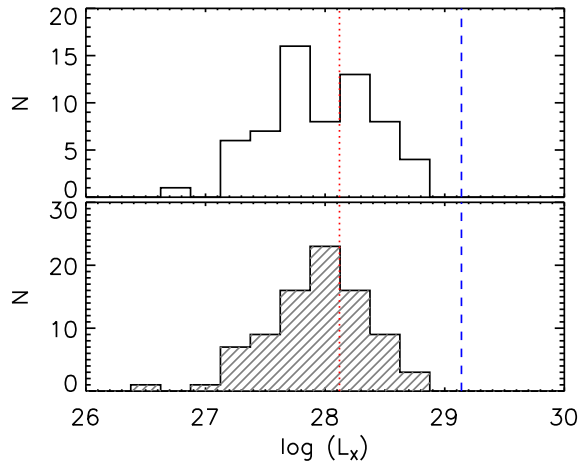


Figure 3. Histogram of the RASS detection limits for the targets within the X-ray (white histogram) and control (grey histogram) samples. Mean L_X values for Pleiades (100 Myr) and Hyades (650 Myr) M-dwarfs as blue dashed and red dotted lines respectively (Micela et al. 1996; Stern et al. 1995).

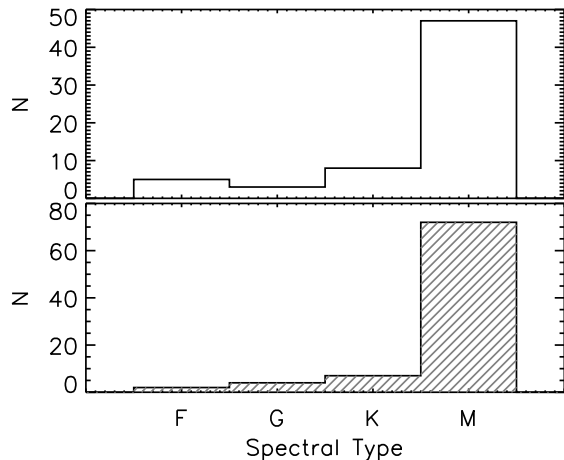


Figure 4. Histogram showing the distribution of the sensitivity of RASS observations to lower-mass companions for targets in the X-ray (white histogram) and control (grey histogram) samples. The evolution of L_X as a function of stellar age was derived from observations of open clusters (Güdel 2004, and references therein).

The distributions of minimum detectable L_X for both samples are shown in Figure 3.

The latest spectral type companion to which the RASS observations are sensitive to depends on the age of the target, derived from theoretical isochrones (Fig. 2 - Marigo et al. 2008), and the X-ray luminosity sensitivity of the observations (Fig. 3). The distribution of this spectral type sensitivity is given in Figure 4. Most of the targets within both samples had RASS observations sensitive to M-type companions and above: 75% of the X-ray sample and 85% of the control sample. Nearly all the RASS observations were sensitive to K-type companions – 87% of the X-ray and 93% of the control sample – and the few remaining targets were sensitive to F- or G-type companions.

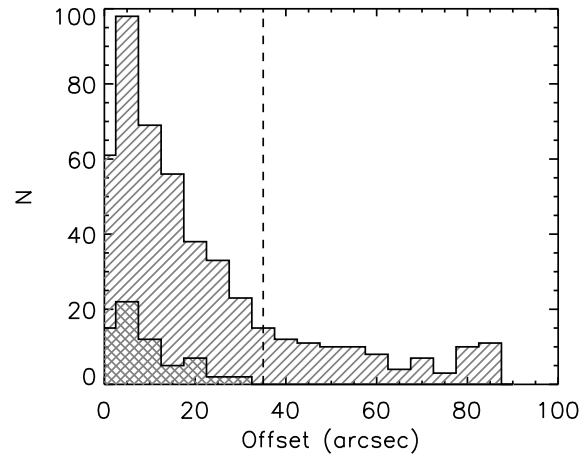


Figure 5. Distribution of *Hipparcos* – *ROSAT* offsets for 479 X-ray detected early-type stars (hatched histogram). These stars have a *ROSAT* source within $90''$ using the same criteria as Huensch et al. (1998a). The tail of the distribution was removed by selecting a more stringent maximum offset of $35''$ (dashed line). The offset distribution for the 63 early-type stars within the X-ray detected sample is overplotted (cross-hatched histogram).

The targets within the X-ray detected sample were chosen based on the presence of a *ROSAT* Bright Source Catalogue (Voges et al. 1999 – BSC) or *ROSAT* Faint Source Catalogue (Voges et al. 2000 – FSC) source within $35''$ of the *Hipparcos* coordinate of each target. As noted in Table 5, 51% are from the Faint Source Catalogue. Previous correlations between BSC sources and optical star catalogues (e.g. Huensch et al. 1998a) have typically used a maximum offset of $90''$ between the catalogue positions, to define an X-ray source. The distribution of the offsets between X-ray source position and *Hipparcos* position is given in Figure 5 and we have applied a more stringent maximum offset cut-off than previous studies, $35''$. All of the A-type stars within the X-ray sample were also identified as X-ray stars in previous studies of X-ray detected A-type stars (e.g. Schröder & Schmitt 2007).

4 OBSERVATIONS

High resolution AO images were obtained for all 148 stars in order to compare the binary statistics of the X-ray and control samples. The data were acquired with several instruments listed in Table 3 – VisIm (Roberts & Neyman 2002) on AEOS, KIR (Doyon et al. 1998) on CFHT, NIRI (Hodapp et al. 2003) on Gemini North, and PHARO (Hayward et al. 2001) on Palomar. The resolution limit λ/D ranged from $0''.05$ for the I_C -band AEOS images to $0''.13$ for the K' CFHT images. The filter used for observations with each instrument is given in Table 3, alongside the corresponding narrowband filter in parentheses. The FWHM of the image cores typically matched the diffraction-limit, due to the high quality AO correction on these bright stars. Given the nearby distances of the targets ($D < 170$ pc), the resolution limit corresponds to projected separations of ~ 10 - 20 AU. The field-of-view ranges from $21''.7 \times 21''.7$ to $35''.6 \times 35''.6$, making binary systems as wide as ~ 3000 AU detectable. The effective field-of-view for the combined science images was increased by dithering the target on the detector. The search range covers the peak of the binary separation distribution of lower mass stars (e.g. Duquennoy & Mayor 1991;

Table 3. Instruments

Telescope	Proposal ID	Dates	<i>N</i>	Filter	λ/D	Field of view	Pixel Scale	North
AEOS	-	02-02-2002 – 03-03-2003	101	I_C	0''.05	24''.6 × 24''.6	0''.048 ± 0''.003	0.0° ± 1.0°
CFHT	2008A-C22	12-06-2008 – 14-06-2008	14	H (FeII)	0''.09	35''.6 × 35''.6	0''.035 ± 0''.0001	-2.4° ± 0.1°
	2008A-C22	13-06-2008 – 14-06-2008	1	K' (H2 ₁₋₀)	0''.13	35''.6 × 35''.6	0''.035 ± 0''.0001	-2.4° ± 0.1°
	2009B-C06	30-08-2009 – 01-09-2009	18	K' (H2 ₁₋₀)	0''.13	35''.6 × 35''.6	0''.035 ± 0''.0001	-2.4° ± 0.1°
	2010A-C14	04-02-2010 – 05-02-2010	29	K' (H2 ₁₋₀)	0''.13	35''.6 × 35''.6	0''.035 ± 0''.0001	-2.4° ± 0.1°
Gemini	GN-2008A-Q-74	18-06-2008 – 24-06-2008	8	K' (Br γ)	0''.06	21''.7 × 21''.7	0''.021 ± 0''.0001	0.5° ± 0.3°
	GN-2008B-Q-119	17-08-2008 – 25-11-2008	26	K' (Br γ)	0''.06	21''.7 × 21''.7	0''.021 ± 0''.0001	0.5° ± 0.3°
	GN-2009B-Q-120	08-09-2009 – 19-12-2009	6	K' (Br γ)	0''.06	21''.7 × 21''.7	0''.021 ± 0''.0001	0.5° ± 0.3°
	GN-2010A-Q-75	10-05-2010	1	K' (Br γ)	0''.06	27''.7 × 21''.7	0''.021 ± 0''.0001	0.5° ± 0.3°
Palomar	-	11-04-2008 – 13-07-2008	13	H (CH ₄ S)	0''.07	25''.4 × 25''.4	0''.025 ± 0''.002	-0.7° ± 0.1°
Palomar	-	11-04-2008 – 13-07-2008	22	K_S (Br γ)	0''.09	25''.4 × 25''.4	0''.025 ± 0''.002	-0.7° ± 0.1°

Fischer & Marcy 1992), important for resolving the bulk of the binary population.

The observing strategy was consistent for all targets. To search for close companions, unsaturated exposures were obtained of each target using either a narrow-band or neutral-density filter. Exposure times ranged from 0.01s to 4.0s, with stacks of 3 to 500 frames. To detect wider, fainter objects approaching the bottom of the Main Sequence, longer exposures in a wide-band filter were recorded with total integration times ranging from 41s to 720s. Details of the filter combinations are given in Table 3 and exposure times of individual targets are listed in Tables 1 and 2. Because of the brightness of the targets, all-sky survey images from 2MASS are saturated over a significant fraction of the separation range covered by the images within this study.

5 DATA ANALYSIS

The science images were processed with standard image reduction steps including dark subtraction, flat fielding, interpolation over bad pixels, and sky subtraction. Alignment of short exposure images was achieved through Gaussian centroiding, while the saturated exposures were aligned by cross-correlating the diffraction spikes (e.g. Lafrenière et al. 2007). To improve the measurable contrast ratios, a radial subtraction was performed on the saturated images to suppress the seeing halo of the central star. Finally, all the processed images were median-combined to increase the signal-to-noise ratio of any detection.

Candidates were identified by visual inspection, and the separation and magnitude difference were measured for each candidate, as reported in Tables 4 and 5. The projected separation between the central star and candidate was calculated from the positions of the centroids of each component in the final median-combined image. The uncertainty of the separation incorporates both the uncertainty in the instrument pixel scale, given in Table 3, and the standard deviation of the measurements from each individual exposure. An estimate of the physical separation in AU was then determined from the *Hipparcos*-derived distance to the primary. The position angle of each candidate was measured based on the instrument field orientation, given in Table 3, and the rotation angle on the sky for all Gemini and a subset of the AEOS data. For data obtained at Palomar and CFHT, there is no instrument or sky rotation. Typically, the total uncertainty is dominated by the measurement uncertainty, however the lack of calibration measurements within some of the observation runs requires a more conservative estimate of the plate scale and angle of true north uncertainty.

The magnitude difference between each candidate and tar-

Table 4. Candidate binary systems within control sample

Designation	Separation arc sec	Position Angle degrees	Magnitude Difference	Filter	Observation Date
HIP2852 B [†]	0.93 ± 0.01	260.6 ± 0.3	5.07 ± 0.03	Br γ	17/10/2008
HIP9487 B	1.83 ± 0.01	266.9 ± 0.2	0.33 ± 0.01	H2 ₁₋₀	01/09/2009
HIP17572 B	3.4 ± 0.1	333.0 ± 1.0	2.54 ± 0.01	I_C	04/02/2002
HIP28360 C	13.9 ± 0.3	155.0 ± 0.1	8.5 ± 0.2	K'	05/02/2010
HIP29711 B	~4.2	~239.7	< 2.5	K'	25/11/2008
HIP35350 B	9.7 ± 0.1	33.8 ± 0.1	3.8 ± 0.1	Br γ	12/04/2008
HIP43570 B	0.66 ± 0.02	310.0 ± 1.0	2.58 ± 0.01	I_C	04/02/2002
HIP44066 B	10.3 ± 0.3	320.9 ± 1.0	5.5 ± 0.2	I_C	01/03/2003
HIP44901 B [†]	26.2 ± 0.1	33.9 ± 0.1	6.0 ± 0.1	K'	05/02/2010
HIP51658 B	16.9 ± 0.04	357.6 ± 0.1	6.0 ± 0.2	K'	04/02/2010
HIP54136 B	7.7 ± 0.3	110.7 ± 1.0	4.6 ± 0.2	I_C	03/03/2003
HIP58510 B [†]	3.2 ± 0.1	218.4 ± 1.0	9.2 ± 0.3	I_C	02/03/2003
HIP68520 Aa [†]	14.4 ± 0.5	41.9 ± 1.0	7.7 ± 0.1	I_C	03/03/2003
HIP69592 B [†]	4.05 ± 0.03	174.5 ± 0.1	5.1 ± 0.1	CH ₄ S	12/07/2008
HIP75043 B	0.26 ± 0.01	227.6 ± 2.0	6.0 ± 0.4	I_C	29/05/2002
HIP84012 B	0.58 ± 0.01	236.0 ± 0.2	0.6 ± 0.1	Br γ	12/04/2008
HIP95081 B [†]	13.1 ± 0.1	16.9 ± 0.3	8.7 ± 0.1	K'	24/06/2008
HIP101300 B	0.26 ± 0.01	241.7 ± 1.3	1.0 ± 0.1	I_C	31/05/2002
HIP109667 B [†]	1.12 ± 0.01	285.2 ± 0.3	4.1 ± 0.1	Br γ	10/09/2008
	1.11 ± 0.01	284.7 ± 0.2	4.2 ± 0.1	H2 ₁₋₀	31/08/2009

[†] - Previously unresolved companion candidate

get star was measured with aperture photometry. Using an aperture of twice the FWHM, the fluxes for the candidate and unsaturated star were measured. If the candidate was only detected in the saturated image, then the comparison flux of the central star was scaled according to the exposure time of the saturated image and the appropriate filter bandpass. The reported magnitude difference uncertainty was estimated as the standard deviation of the values from each processed image before combination. Using the magnitudes of the target from the *Hipparcos* and 2MASS (Cutri et al. 2003) source catalogues, the apparent magnitude of the candidate was determined. An estimate of the physical properties of both primary and candidate companion was made using a combined set of theoretical solar-metallicity isochrones (Marigo et al. 2008; Baraffe et al. 1998). Each target was plotted on a colour-magnitude diagram (Fig. 2) from which an estimate of the age was derived. Estimated colours and bolometric luminosities were obtained for the companion candidates based on the measured magnitude difference, using an isochrone of the same age as the primary.

6 RESULTS

6.1 Detections

Among the 148 targets, a total of 68 candidate companions were imaged around 59 members of the total sample. One-third of the candidate companions, 23 systems, are newly resolved. The binary angular separations range from 0''.3 to 26''.2, and the magnitude differences range from 0.3 to 11.9, corresponding to spectral types of mid-A to late-M for associated companions. The measured magnitude difference of the candidates is plotted as a function of sep-

Table 5. Candidate binary systems within X-ray detected sample

Designation	Separation <i>arc sec</i>	Position Angle <i>degrees</i>	Magnitude Difference	Filters	Observation Date	Estimated $V - I$	Estimated $\log(L_X / L_{\text{Bol}})$
5310 B [†] *	0.36 ± 0.01	175.3 ± 0.3	3.91 ± 0.04	Br γ	16/10/2008	1.98	-3.01
9480 B*	0.67 ± 0.01	297.3 ± 0.2	1.18 ± 0.02	H2 ₁ –0	01/09/2008	0.64	-4.24
11569 B*	2.77 ± 0.01	230.0 ± 0.2	1.60 ± 0.02	H2 ₁ –0	05/02/2010	0.64	-4.32
11569 C	7.22 ± 0.01	115.3 ± 0.1	1.98 ± 0.01	H2 ₁ –0	05/02/2010	0.75	-4.08
13133 C [†]	~6.6	~70.5	< 1.9	K'	14/11/2008	0.86	-3.00
13133 D [†] *	3.87 ± 0.03	229.8 ± 0.3	9.4 ± 0.3	K'	14/11/2008	4.94	1.16
17608 Ab [†]	0.25 ± 0.02	111.0 ± 1.1	4.0 ± 0.4	I _C	04/02/2002	0.54	-4.32
17923 B	3.1 ± 0.1	232.3 ± 1.0	2.66 ± 0.01	I _C	03/02/2002	0.65	-3.29
17923 Ca	9.7 ± 0.3	233.7 ± 1.0	2.8 ± 0.1	I _C	03/02/2002	0.68	-3.23
17923 Cb	10.2 ± 0.3	235.0 ± 1.0	4.5 ± 0.2	I _C	03/02/2002	1.08	-2.52
19949 B [†]	13.5 ± 0.4	146.9 ± 1.0	7.3 ± 0.3	I _C	05/02/2002	1.88	-2.63
20648 B	1.7 ± 0.1	337.9 ± 1.0	3.12 ± 0.02	I _C	04/02/2002	0.80	-4.84
	1.80 ± 0.01	341.4 ± 0.1	2.55 ± 0.01	H2 ₁ –0	04/02/2010		
22287 Ab*	0.46 ± 0.01	41.6 ± 1.2	3.8 ± 0.1	I _C	05/02/2002	1.13	-4.41
22287 B*	13.2 ± 0.5	238.7 ± 1.0	5.5 ± 0.2	I _C	05/02/2002	1.82	-3.78
23179 B*	~4.7	~4.0	< 2.6	K'	15/11/2008	1.12	-2.81
24019 B*	~11.2	~26.1	< 2.4	I _C	04/02/2002	0.86	-4.38
28614 BaBb*	0.40 ± 0.01	22.1 ± 0.3	1.27 ± 0.01	K'	19/12/2009	0.27	-5.36
29997 B [†]	8.47 ± 0.05	218.1 ± 0.4	6.8 ± 0.1	K'	01/09/2009	2.43	-2.16
30419 B*	12.20 ± 0.04	29.0 ± 0.2	1.72 ± 0.03	H2 ₁ –0	01/09/2009	0.65	-4.95
39095 B*	5.3 ± 0.2	65.8 ± 1.0	9.5 ± 0.7	I _C	02/02/2002	2.32	-2.63
39847 Aa [†]	4.6 ± 0.2	114.0 ± 1.0	9.5 ± 0.5	I _C	02/02/2002	2.39	-2.26
42313 Ab [†]	2.6 ± 0.1	265.1 ± 1.0	6.6 ± 0.2	I _C	04/02/2002	1.79	-3.08
	2.6 ± 0.1	262.7 ± 3.1	7.3 ± 0.2	I _C	01/03/2003		
44127 B*	2.35 ± 0.02	76.6 ± 0.1	4.22 ± 0.02	Br γ	12/04/2008	2.08	-3.55
	2.40 ± 0.01	78.8 ± 0.1	4.36 ± 0.02	H2 ₁ –0	05/02/2010		
44127 C*	1.94 ± 0.02	79.8 ± 0.1	4.26 ± 0.02	Br γ	12/04/2008	2.09	-3.53
	1.92 ± 0.01	87.2 ± 0.1	4.30 ± 0.02	H2 ₁ –0	05/02/2010		
45688 B*	2.5 ± 0.1	222.6 ± 1.0	1.64 ± 0.03	I _C	06/02/2002	0.48	-4.79
	2.60 ± 0.02	224.0 ± 0.1	1.2 ± 0.1	Br γ	12/04/2008		
51200 B*	2.41 ± 0.01	304.1 ± 0.1	3.08 ± 0.01	H2 ₁ –0	04/02/2010	1.42	-3.63
52913 B*	2.3 ± 0.1	13.8 ± 1.1	0.31 ± 0.01	I _C	02/03/2003	0.31	-5.13
62394 Ab [†] *	3.2 ± 0.1	348.8 ± 1.4	7.0 ± 0.2	I _C	29/05/2002	2.16	-2.37
65241 B [†] *	0.34 ± 0.02	41.7 ± 3.2	4.3 ± 0.4	I _C	03/03/2003	1.40	-3.16
65477 B*	1.07 ± 0.01	209.0 ± 0.1	5.6 ± 0.1	CH ₄ S	11/04/2008	2.19	-3.46
66249 B	1.81 ± 0.01	154.4 ± 0.1	6.4 ± 0.1	H2 ₁ –0	05/02/2010	2.45	-3.18
66727 B	4.4 ± 0.1	338.5 ± 1.2	2.95 ± 0.02	I _C	03/03/2003	0.74	-3.72
76376 C [†] *	9.6 ± 0.4	350.1 ± 1.0	11.9 ± 0.3	I _C	29/05/2002	3.6	-1.52
76878 B*	2.3 ± 0.1	53.4 ± 1.7	7.3 ± 0.2	I _C	29/05/2002	2.24	-2.31
	2.4 ± 0.02	86.4 ± 0.1	5.1 ± 0.4	K _S	13/07/2008		
80628 B*	0.67 ± 0.01	22.6 ± 0.1	2.26 ± 0.03	Br γ	12/04/2008	0.90	-3.78
82321 B	1.82 ± 0.01	34.1 ± 0.1	2.2 ± 0.1	CH ₄ S	12/07/2008	0.77	-4.66
82321 C	2.06 ± 0.02	38.4 ± 0.1	2.69 ± 0.03	CH ₄ S	12/07/2008	0.90	-4.39
87045 B*	0.32 ± 0.01	144.1 ± 1.1	2.45 ± 0.04	I _C	29/05/2002	0.62	-3.71
88771 B*	24.83 ± 0.06	297.6 ± 0.1	5.2 ± 0.1	K'	05/02/2010	2.18	-3.83
88771 D	24.20 ± 0.06	48.4 ± 0.1	8.1 ± 0.1	K'	05/02/2010	3.40	-2.53
91971 B	23.28 ± 0.07	51.3 ± 0.2	9.7 ± 0.2	K'	13/06/2008	4.27	-0.33
93747 B	7.27 ± 0.02	47.0 ± 0.2	4.88 ± 0.02	FeII	13/06/2008	1.99	-3.23
98103 C [†] *	2.8 ± 0.1	184.7 ± 0.2	4.7 ± 0.1	K'	18/06/2008	2.05	-2.96
102033 B*	0.72 ± 0.02	345.4 ± 1.1	2.36 ± 0.01	I _C	31/05/2002	0.72	-4.62
106711 B [†]	6.98 ± 0.04	58.1 ± 0.3	8.5 ± 0.1	K'	08/09/2008	3.00	-2.14
109521 B [†] *	9.98 ± 0.06	241.3 ± 0.3	8.1 ± 0.1	K'	08/09/2008	3.27	-1.18
110787 B [†] *	0.29 ± 0.01	211.1 ± 0.6	4.3 ± 0.1	Br γ	17/09/2008	2.03	-3.18
117452 Ba [†] *	3.7 ± 0.1	237.3 ± 0.4	3.48 ± 0.04	H2 ₁ –0	30/08/2009	1.61	-3.01
117452 Bb [†] *	3.5 ± 0.1	238.5 ± 0.5	3.7 ± 0.1	H2 ₁ –0	30/08/2009	1.73	-2.90

† - Previously unresolved companion candidate

* - Companion candidate falls within RASS error ellipse

Table 6. Results Summary

	Total Field-of-View		RASS Error Ellipse Search Area	
	X-Ray	Control	X-Ray	Control
A8 – M9 Companion ¹	60 ⁺⁶ ₋₆ %	20 ⁺⁵ ₋₄ %	43 ⁺⁶ ₋₆ %	12 ⁺⁴ ₋₃ %
B6 – A7 Companion	2 ⁺⁴ ₋₁ %	2 ⁺³ ₋₁ %	3 ⁺⁴ ₋₁ %	2 ⁺³ ₋₁ %
No Resolved Companion	38 ⁺⁶ ₋₆ %	78 ⁺⁴ ₋₅ %	56 ⁺⁶ ₋₆ %	86 ⁺³ ₋₄ %

¹ - Expected spectral type based on measured magnitude difference and assuming the same distance as the target.

aration in Figure 6. Properties of the companion candidates in the X-ray and control samples are listed in Tables 4 and 5, respectively. Candidate companions are limited to those with less than 5% probability of being a background object, based on the star density analysis described in §6.3.

6.2 Detection limits

The sensitivity to companions varies with angular separation from the central star due to the significant residual halo from the bright targets. Detection limits for each image are quantified by determining the flux level in a 5×5 pixel aperture that would produce a

signal 5 σ above the noise within the aperture. The median magnitude difference sensitivity curve for each instrument is plotted in Figure 6. Since the data were obtained at several wavelengths, the bottom of the Main Sequence corresponds to a different magnitude difference for each instrument. For an A0 primary, a companion at the bottom of the Main Sequence would have an absolute magnitude of 14.3 at I_C, 10.5 at H, and 10.2 at K_S at an age of 700 Myr. The infrared data obtained at CFHT and Gemini are sensitive to the bottom of the Main Sequence at separations beyond ~ 2''. The achieved contrast for the Palomar data was less due to the shorter exposure times, and reached a companion mass limit of 0.12 M_☉ to 0.2 M_☉, depending on the age of the target. The AEOS data have a sensitivity limit to companions ranging from 0.08 M_☉ to 0.1 M_☉.

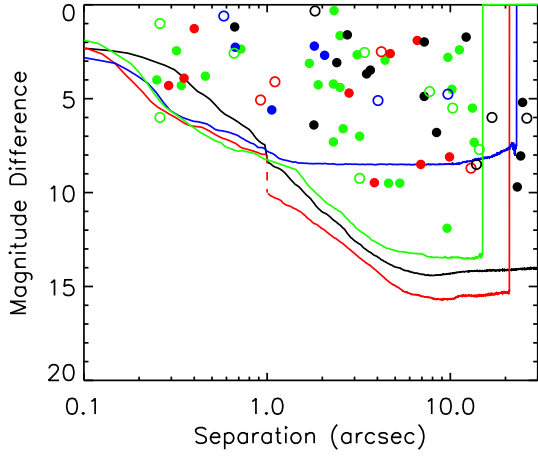


Figure 6. The magnitude difference of the candidate companions detected within this study as a function of angular separation from the central star. Filled and open circles represent companions within the X-ray and control samples, respectively. Colours represent each of the instruments used: AEOS (green), CFHT (black), Gemini (red), Palomar (blue). Over-plotted are the detection limits for each instrument (see §6.2). The dashed portion of the Gemini sensitivity curve represents the edge of the field of view for the unsaturated exposures.

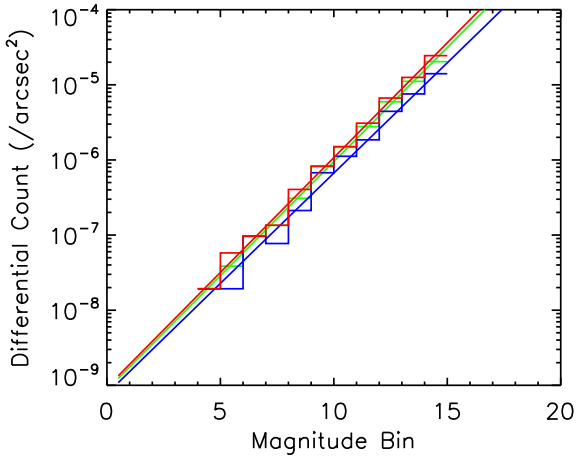


Figure 7. Histogram of differential source counts and corresponding logarithmic fits within the 2MASS source catalogue in the vicinity of HIP57646 in J , H and K_S filters (blue, green and red respectively).

The sensitivity to companions for both the X-ray and control samples is similar, making the difference between the two measured binary frequencies a valid test of the companion hypothesis.

6.3 Probability of chance superpositions

An estimate of the probability of each companion candidate being an optical binary was made based on the local stellar densities for each target, measured from the 2MASS source catalogue. The number of sources within a $2^\circ \times 2^\circ$ box of each target was determined in magnitude bins 1 magnitude in width from 0–14 mag for the J , H , and K_S bandpasses. An example plot of this differential source

count per area is given in Figure 7. A power law fit was applied to the counts such that

$$N = \pi \rho^2 10^{b+am} \quad (1)$$

where N is the number of sources within a separation ρ from the target, with an apparent magnitude brighter than m , expressed as a function of the two fit parameters a , the gradient, and b , the intercept. For the I_C band observations obtained at the AEOS, we have approximated the local stellar density using the J band 2MASS data. Candidates with $N > 0.05$ were assumed to be a background object, and not counted for any aspect of this study – a total of 492 candidates were rejected through this process. To compare the stellar density across the samples, Tables 1 & 2 give the number of objects brighter than 14th magnitude expected per square arcminute in the vicinity of each target. In order to prove physical association of the companion candidates which satisfy this criterion, a second epoch measurement will be required.

7 DISCUSSION

7.1 Multiplicity comparison

The frequency of multiple systems in the X-ray and control sample was determined by two methods. In the first calculation, the total field-of-view of each observation was used, and, in the second calculation, the search area was restricted to the RASS position error box. For each approach, candidate companions with a small magnitude difference, consistent with a spectral type in the B6–A7 range, were excluded from the X-ray companion hypothesis test and are listed separately in Table 6. This criterion of a companion capable of generating X-rays eliminated one binary companion from the X-ray sample and two companions from the control sample. All multiple systems considered also satisfied the background object probability of $< 5\%$, as described in §6.3.

Considering the total field-of-view of the combined dithered observations, candidates satisfying the magnitude and background probability criteria were included in the multiple frequency measurement. Among the X-ray sample, $60^{+6}_{-6}\%$ were multiple, compared to $20^{+5}_{-4}\%$ for the control sample – a difference of $40 \pm 8\%$, a 5σ result. These and subsequent reported errors are estimated from a binomial distribution (e.g. Burgasser et al. 2003). Spectroscopic binaries – unresolved with these observations – constitute a significant fraction of both samples ($\sim 15\%$, Pourbaix et al. 2004). This estimate represents a lower limit on the frequency since the sample of stars observed with the radial velocity monitoring is not known, and the large $v \sin i$ of the primary and less massive unseen companions make such observations challenging. These spectroscopically resolved binaries are not considered within our statistics.

The multiplicity of the X-ray sample was also measured by considering only companion candidates that were located within the confines of the RASS error ellipse. For each target, the AO data covered a portion of the RASS error ellipse ranging from 25 to 100 percent. This additional restriction lowered the multiple frequency to $43^{+6}_{-6}\%$. To determine a comparable frequency for the control sample, a series of companion searches were performed by randomly assigning the RASS-optical offset and corresponding error ellipse of an X-ray target to a control target and determining the number of candidate companions which fall within the error ellipse. Based on a large number of simulations (100,000), the frequency of multiples was estimated as $12^{+4}_{-3}\%$. These two frequencies are different by $31 \pm 7\%$, a 4σ result.

A summary of the multiplicity calculations is given in Table

6. The high statistical significance of the difference in frequencies for the X-ray and control samples provides strong support of the companion hypothesis as an explanation of the X-ray detection of B6–A7 stars. Further evidence for individual systems with separations of a few arcsecond could be provided by high resolution *Chandra* observations which would have the pointing accuracy to assign the X-ray flux to the companion unambiguously. One target, Merope in the Pleiades, was observed with the high resolution mode of *Chandra*, but the binary separation is only $0''.25$, making the discrepancy between the *Chandra* and 2MASS coordinates ambiguous in this case. Targets within the X-ray sample for which no companions have been resolved will make prime targets for future interferometric and spectroscopic study in a search for lower-mass companions with angular separations low enough to render them undetectable with AO observations.

7.2 ROSAT positional uncertainty

Previous studies of the unexplained X-ray detection of early-type stars (e.g. Schröder & Schmitt 2007) have used the same definition of an X-ray detected early-type star as presented by Huensch et al. (1998a) – any X-ray source within $90''$ of an optical source can be attributed to the optical source. This value was based on estimating the frequency of false attribution by means of a Monte Carlo simulation, and was selected at the radius at which the probability of correctly attributing an X-ray source is ~ 50 percent. A significantly lower offset of $25''$ was calculated by Voges et al. (1999) from a correlation of the *Tycho* catalogue and *ROSAT* Bright Source Catalogue positions, a radius within which 90 percent of the optical targets have an X-ray source attributed. This measurement represents the empirical positional uncertainty of the RASS source catalogue positions.

The sample investigated within this study was initially selected in the same manner as Huensch et al. (1998a) – using a maximum offset of $90''$. The tail of the offset distribution was removed by applying a more stringent maximum offset at $35''$, as described in §3. Variations in the field-of-view size between instruments caused the coordinates of the X-ray source given within the RASS to be outside of the field-of-view within a small subset of the observations. In order to investigate any biases this may have had upon the results presented previously, the sample was further restricted to only include those targets for which the RASS source position was within the field-of-view and at least 50 percent of the RASS error ellipse was covered – a total of 45 stars. For this sample a marginally higher frequency of companions located within the RASS error ellipse was recorded, $53^{+7}_{-7}\%$, reinforcing the result obtained with the unrestricted sample.

7.3 Comparison of measured and expected X-ray luminosities

7.3.1 Candidate companions with measured colours

Several of the candidate companions to X-ray targets have a measured $I - K$ colour from this study, and are plotted in Figure 8. The colour provides additional information to estimate the spectral type of the object and to test further the capacity of the second object to generate X-ray emission. The three systems with colours are: (1) HIP 20648, (2) HIP 45688, and (3) HIP 76878. The $I - K$ colours of the candidate companions are all consistent with X-ray emitting companions: 0.71 ± 0.05 or late F-/early G-type for HIP 20648 B,

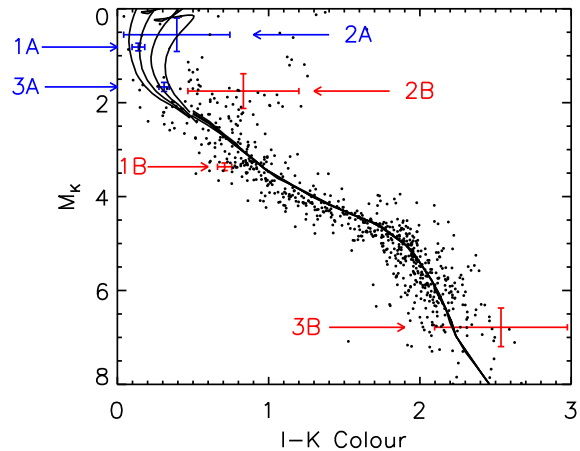


Figure 8. A colour-magnitude diagram of 792 nearby Gliese stars. Overplotted are four theoretical isochrones of ages $\log t = 8.7, 8.8, 8.9, 9.0$ (Marigo et al. 2008; Baraffe et al. 1998). Three of the targets within the X-ray sample are plotted in blue: HIP 20648 (1), HIP 45688 (2) and HIP 76878 (3). The corresponding resolved companions for each primary are shown in red.

0.83 ± 0.37 or mid G-type for HIP 45688 B, and 2.54 ± 0.44 or late M-type for HIP 76878 B.

With the assumption of a distance and age equivalent to the primary distance, the X-ray luminosity associated with the *ROSAT* detection can be checked for consistency with the spectral type. The position on the colour-magnitude diagram for each primary star and its imaged candidate companion is given in Figure 8, assuming the distance to each component is the same. Each case is examined individually, and the colour and proper motion measurements clearly support the assignment of the X-ray emission to the candidate companion in two cases, while one case remains uncertain.

The theoretical isochrone that best fits the first target, HIP 20648A, corresponds to an age of ~ 650 Myr, and the candidate companion position in Figure 8 is as expected for an associated companion. The companion X-ray luminosity is $\log L_X = 28.71$, and this value falls between the X-ray luminosities of Hyades F- and G-type stars. The assessment of the second target, HIP 45688, is complicated by the presence of a known close companion to the imaged candidate companion ($\rho \sim 0''.06$ – McAlister et al. 1993), unresolved in the current data. The composite colour and magnitude of the BaBb system appear to be more luminous than expected for an object at the 630 Myr age estimated for the primary, even if the pair is an equal magnitude binary. The X-ray luminosity of BaBb would be $\log L_X = 29.43$, significantly higher than younger G-type stars in the Hyades. For the final system, HIP 76878, the best fit age is 700 Myr, similar to the Hyades. The X-ray luminosity of the candidate companion is $\log L_X = 29.26$, if the distance is equal to that of HIP 76878. This X-ray level is higher than observed X-ray luminosities of M-dwarfs of similar age within the Hyades (Stern et al. 1995). In this case, the time baseline between the two observations also reveals a significant motion of the candidate relative to the primary on a trajectory different from both a background object and a bound companion. The presence of a foreground M-dwarf in a chance superposition with HIP 76878 explains this discrepant proper motion, the red colour of the object, and the unusually high X-ray luminosity.

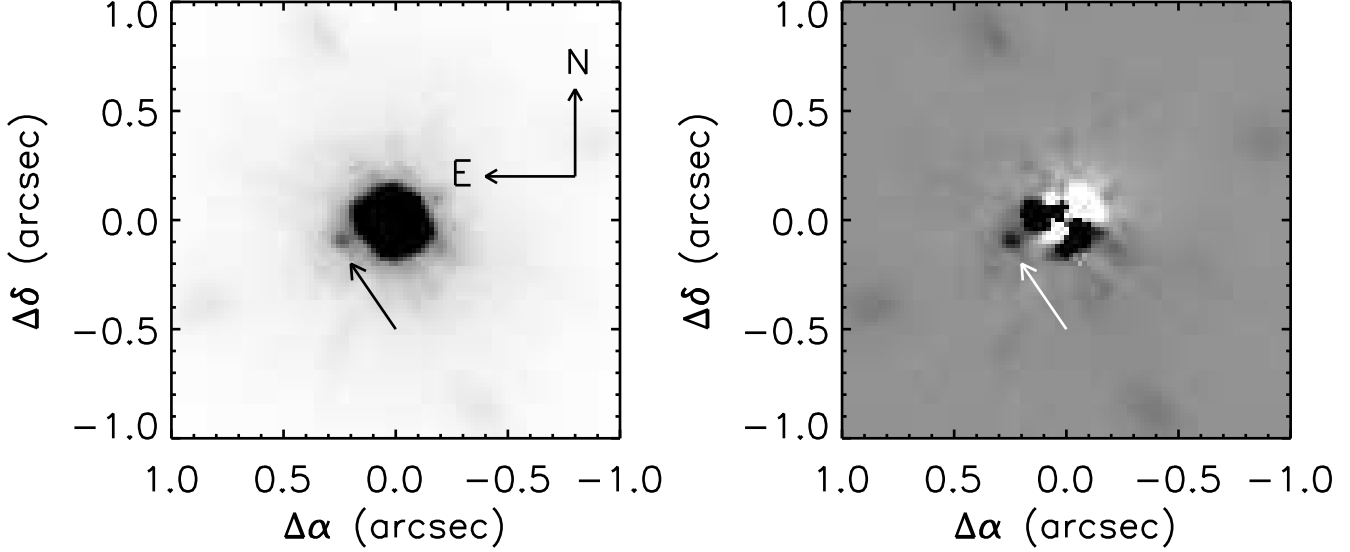


Figure 9. A sub-arcsecond companion candidate is resolved around HIP17608 (Merope), a member of the Pleiades cluster. A faint ($\Delta I = 4.0 \pm 0.4$) companion candidate at $\rho = 0''.25$, $\theta = 110^\circ$ is visible within the median combined image of the 500, 0.048 second unsaturated exposures (*left panel*). The scale is linear from 0 (white) to 45 (black). After radial subtraction the object becomes more prominent (*right panel*), with a linear scale between -15 and 20.

7.3.2 Candidate companions in open clusters

A subset of the X-ray detected targets with imaged candidate companions are members of stellar clusters. HIP 17608 and HIP 17923 are Pleiades members, while HIP 20648 is a Hyades member. Extensive X-ray population studies of both the Pleiades (e.g. Micela et al. 1985; Stauffer et al. 1994; Daniel et al. 2002) and the Hyades (e.g. Micela et al. 1988; Stern et al. 1995) have been conducted with *Einstein* ROSAT and *Chandra*, providing comparison X-ray luminosities to test the likelihood that the candidate companions are responsible for the detected X-ray emission.

The candidate companion to HIP 17608 (Merope in the Pleiades) with $0''.25$ separation is shown in Figure 9. With a magnitude difference of $\Delta I_C = 4.0 \pm 0.4$, the second object is a mid F-type star if associated. Assuming a distance to the Pleiades of 133 pc (Pan et al. 2004), the X-ray luminosity for the HIP 17608 system is $\log L_X = 29.91$. The typical X-ray luminosity of F-dwarfs within the Pleiades is estimated to be $\log L_X \sim 29.43 \pm 0.29$ (Stauffer et al. 1994), indicating that the companion to HIP17608, if associated, is on the upper limit of X-ray activity for this class of star.

For the second Pleiades member, the observations resolve three of the companions (B,Ca,Cb) within the HIP17923 quintuple system. Based on the measured magnitude differences, we estimate the mass of the components as follows: B – $1.2 \pm 0.1 M_\odot$ (mid F-type), Ca – $1.2 \pm 0.1 M_\odot$ (mid F-type), Cb – $0.9 \pm 0.1 M_\odot$ (mid G-type). Deeper X-ray observations of the Pleiades (Micela et al. 1999) revealed an estimated X-ray luminosity of $\log L_X = 30.08$ for this system. If the X-ray counts were distributed evenly between the three later-type companions resolved within our AO images, the individual X-ray luminosities would be $\log L_X \sim 29.6$, similar to G- and F-type Pleiades members (Stauffer et al. 1994).

The final cluster X-ray target with a resolved companion is the Hyades member HIP 20648. As described in §7.2, the candidate

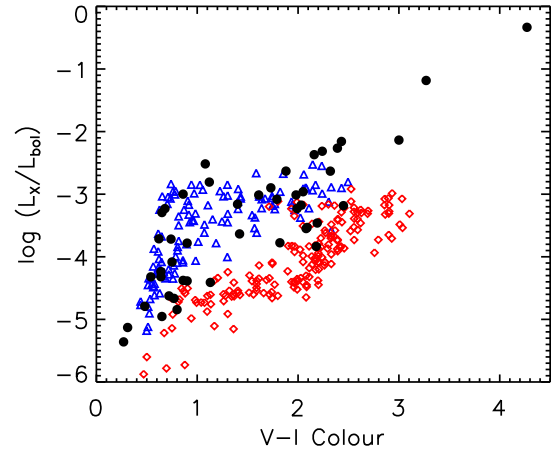


Figure 10. The ratio of X-ray to bolometric luminosity is plotted as a function of colour for the candidates resolved within this study. The majority of candidates are constrained by the Pleiades (blue triangles) and Hyades (red diamonds) members, representing the two age extremes of the sample.

companion also has a measured I-K colour consistent with a late F-/early G-type star, and the X-ray luminosity assigned to the target is consistent with a Hyades G-type star (Stern et al. 1995).

7.3.3 Remaining candidate companions

For the remaining candidate companions, an estimate of the ratio of X-ray to bolometric luminosity can be made under the assumption that the candidate is a physical companion at the same distance. From the absolute magnitude, the $V - I$ colour and bolometric lu-

minosity were inferred from theoretical isochrones (Baraffe et al. 1998). The ratios of the observed X-ray luminosity to the estimated bolometric luminosity (L_X/L_{bol}) are plotted as a function of $V - I$ colour in Figure 10, with Pleiades and Hyades members (Zuckerman & Song 2004) overplotted as reference populations spanning the age range of the sample.

All but two of the candidates are within the region bound by the ~ 100 Myr Pleiades and ~ 650 Myr Hyades members. Uncertainty exists on both axes since both the $V - I$ colour and bolometric luminosity are estimated from theoretical isochrones, assuming the distance. Future observations to accurately determine the colour of these candidates will provide a more robust estimate of the bolometric luminosity. The two outlying candidates shown in Figure 10 have unphysical high luminosity ratios, significantly higher than the observed luminosity ratios of late M-type stars (e.g. Pizzolato et al. 2003). In these two cases, additional unresolved companions, or background X-ray sources, present a more feasible explanation for the detected X-ray flux. The rate of false-detections, 2/49, corresponds to the 5% contamination introduced through the statistical method applied to the candidates to remove background sources, as described in §6.3.

8 SUMMARY

In summary, a total of 148 stars with spectral types in the range B6–A7 and distances of < 200 pc have been observed with AO-equipped cameras on 3.8m–8m telescopes. The high resolution images were sensitive to companions with angular separations from $\sim 0''.3$ to $26''.2$ and magnitude differences extending to ~ 14 mag. A total of 68 candidate companions to 59 targets were resolved, and the frequency of multiple systems was measured to be substantially higher for the X-ray detected sample. The high frequency of multiples, $43^{+6}_{-6}\%$, compared to $12^{+4}_{-3}\%$ for the control sample is different by 4σ and provides strong evidence that the source of the X-ray emission is the candidate companion. The X-ray detected stars with no resolved companion make ideal candidates for future interferometric observations, as this study has shown that the X-ray detection is indicative of the presence of an unresolved companion, and interferometry can resolve binaries below the resolution of the adaptive optics data presented here.

For three candidate companions to X-ray targets, the $I - K$ colour was also measured, and the colours are consistent with late F- to late M-type stars, supporting the identification of the second object as the X-ray source in two cases. Among the X-ray targets with candidate companions, there are also three cluster members, and the known age, distance, and cluster X-ray properties enabled a further test of the companion X-ray luminosity with other cluster members. In each case, the companions – if associated – would have an X-ray luminosity similar to, or on the upper range of, cluster stars with similar magnitude. Follow-up observations of the X-ray targets with candidate companions using *Chandra* would provide the angular resolution in the X-ray band necessary to confirm the second object as the true source of the X-ray emission.

ACKNOWLEDGEMENTS

We gratefully acknowledge several sources of funding. R. J. DR. and J. B. (ST/F 007124/1) are funded through studentships from the Science and Technology Facilities Council (STFC). This work

was initiated with a grant awarded to J. P. from the Air Force Office of Scientific Research (AFOSR) for the AEOS component and completed with a grant from the STFC (ST/F003277/1). Funding for collaborative visits was provided by the CONSTELLATION EC Research Training Network. Portions of this work were performed under the auspices of the U.S. Department of Energy by Lawrence Livermore National Laboratory in part under Contract W-7405-Eng-48 and in part under Contract DE-AC52-07NA27344, and also supported in part by the NSF Science and Technology CfAO, managed by the UC Santa Cruz under cooperative agreement AST 98-76783. This work was supported, through J. R. G., in part by University of California Lab Research Program 09-LR-118057-GRaj and NSF grant AST-0909188. We thank LLNL summer students C. White (US Air Force Academy) and S. Kost (Carnegie Mellon University) who assisted with obtaining a subset of the data and some of the early analysis. This research has made use of the SIMBAD and VizieR databases, operated at CDS, Strasbourg, France. This publication makes use of data products from the Two Micron All Sky Survey, which is a joint project of the University of Massachusetts and the Infrared Processing and Analysis Center/California Institute of Technology, funded by the National Aeronautics and Space Administration and the National Science Foundation. This research has made use of the Washington Double Star Catalog maintained at the U.S. Naval Observatory. We thank the referee for the helpful comments during the review process.

REFERENCES

- Baraffe I., Chabrier G., Allard F., Hauschildt P. H., 1998, *A&A*, 337, 403
- Berghofer T. W., Schmitt J. H. M. M., 1994, *Astronomy and Astrophysics* (ISSN 0004-6361), 292, L5
- Burgasser A. J., Kirkpatrick J. D., Reid I. N., Brown M. E., Miskey C. L., Gizis J. E., 2003, *ApJ*, 586, 512
- Chabrier G., Baraffe I., 1997, *A&A*, 327, 1039
- Chabrier G., Küker M., 2006, *A&A*, 446, 1027
- Cutri R., Skrutskie M., Dyk S. V., Beichman C., Carpenter J., Chester T., Cambresy L., Evans T., Fowler J., Gizis J., Howard E., Huchra J., Jarrett T., 2003, *The IRSA 2MASS All-Sky Point Source Catalog*, NASA/IPAC Infrared Science Archive. <http://irsa.ipac.caltech.edu/applications/Gator/>, -1,
- Daniel K. J., Linsky J. L., Gagné M., 2002, *ApJ*, 578, 486
- De-Pontieu B., McIntosh S. W., Carlsson M., Hansteen V. H., Tarbell T. D., Schrijver C. J., Title A. M., Shine R. A., Tsuneta S., Katsukawa Y., Ichimoto K., Suematsu Y., Shimizu T., Nagata S., 2007, *Science*, 318, 1574
- Doyon R., Nadeau D., Vallee P., Starr B. M., Cuillandre J. C., Beuzit J.-L., Beigbeder F., Brau-Nogue S., 1998, *Proc. SPIE Vol.* 3354, 3354, 760
- Duquenois A., Mayor M., 1991, *A&A*, 248, 485
- Feldmeier A., Puls J., Pauldrach A. W. A., 1997, *A&A*, 322, 878
- Fischer D. A., Marcy G. W., 1992, *ApJ*, 396, 178
- Giampapa M. S., Prosser C. F., Fleming T. A., 1998, *Astrophysical Journal* v.501, 501, 624
- Güdel M., 2004, *A&AR*, 12, 71
- Hayward T. L., Brandl B., Pirger B., Blacken C., Gull G. E., Schoenwald J., Houck J. R., 2001, *The Publications of the Astronomical Society of the Pacific*, 113, 105
- Hinkley S., Oppenheimer B. R., Brenner D., Zimmerman N., Roberts L. C., Parry I. R., Soummer R., Sivaramakrishnan A., Simon M., Perrin M. D., King D. L., Lloyd J. P., Bouchez A.,

- Roberts J. E., Dekany R., Beichman C., Hillenbrand L., Burruss R., Shao M., Vasisht G., 2010, *ApJ*, 712, 421
- Hodapp K. W., Jensen J. B., Irwin E. M., Yamada H., Chung R., Fletcher K., Robertson L., Hora J. L., Simons D. A., Mays W., Nolan R., Bec M., Merrill M., Fowler A. M., 2003, *The Publications of the Astronomical Society of the Pacific*, 115, 1388
- Hoffleit D., 1964, New Haven
- Hubrig S., Mignant D. L., North P., Krautter J., 2001, *A&A*, 372, 152
- Huélamo N., Neuhauser R., Stelzer B., Supper R., Zinnecker H., 2000, *A&A*, 359, 227
- Huensch M., Schmitt J. H. M. M., Voges W., 1998a, *A&AS*, 127, 251
- Huensch M., Schmitt J. H. M. M., Voges W., 1998b, *A&AS*, 132, 155
- Jess D. B., Mathioudakis M., Erdélyi R., Crockett P. J., Keenan F. P., Christian D. J., 2009, *Science*, 323, 1582
- Lafrenière D., Doyon R., Marois C., Nadeau D., Oppenheimer B. R., Roche P. F., Rigaut F., Graham J. R., Jayawardhana R., Johnstone D., Kalas P. G., Macintosh B., Racine R., 2007, *ApJ*, 670, 1367
- Lucy L. B., White R. L., 1980, *ApJ*, 241, 300
- McAlister H. A., Mason B. D., Hartkopf W. I., Shara M. M., 1993, *Astronomical Journal* (ISSN 0004-6256), 106, 1639
- Mamajek E. E., Kenworthy M. A., Hinz P. M., Meyer M. R., 2010, *AJ*, 139, 919
- Marigo P., Girardi L., Bressan A., Groenewegen M. A. T., Silva L., Granato G. L., 2008, *A&A*, 482, 883
- Micela G., Sciortino S., Harnden F. R., Kashyap V., Rosner R., Prosser C. F., Damiani F., Stauffer J., Caillault J.-P., 1999, *A&A*, 341, 751
- Micela G., Sciortino S., Kashyap V., Harnden F. R., Rosner R., 1996, *Astrophysical Journal Supplement* v.102, 102, 75
- Micela G., Sciortino S., Serio S., Vaiana G. S., Bookbinder J., Golub L., Harnden F. R., Rosner R., 1985, *ApJ*, 292, 172
- Micela G., Sciortino S., Vaiana G. S., Schmitt J. H. M. M., Stern R. A., Harnden F. R., Rosner R., 1988, *ApJ*, 325, 798
- Owocki S. P., Castor J. I., Rybicki G. B., 1988, *ApJ*, 335, 914
- Pan X., Shao M., Kulkarni S. R., 2004, *Nature*, 427, 326
- Patterson J., Raymond J. C., 1985, *ApJ*, 292, 535
- Pizzolato N., Maggio A., Micela G., Sciortino S., Ventura P., 2003, *A&A*, 397, 147
- Pourbaix D., Tokovinin A. A., Batten A. H., Fekel F. C., Hartkopf W. I., Levato H., Morrell N. I., Torres G., Udry S., 2004, *A&A*, 424, 727
- Randich S., 2000, *Stellar Clusters and Associations: Convection*, 198, 401
- Roberts L. C., Neyman C. R., 2002, *The Publications of the Astronomical Society of the Pacific*, 114, 1260
- Schatzman E., 1949, *Annales d'Astrophysique*, 12, 203
- Schmitt J. H. M. M., Golub L., Harnden F. R., Maxson C. W., Rosner R., Vaiana G. S., 1985, *ApJ*, 290, 307
- Schmitt J. H. M. M., Micela G., Sciortino S., Vaiana G. S., Harnden F. R., Rosner R., 1990, *ApJ*, 351, 492
- Schmitt J. H. M. M., Zinnecker H., Cruddace R., Harnden F. R., 1993, *ApJ*, 402, L13
- Schröder C., Schmitt J. H. M. M., 2007, *A&A*, 475, 677
- Schwarzschild M., 1948, *ApJ*, 107, 1
- Shapiro S. L., Lightman A. P., Eardley D. M., 1976, *ApJ*, 204, 187
- Shatsky N., Tokovinin A., 2002, *A&A*, 382, 92
- Simon T., Drake S. A., Kim P. D., 1995, *PASP*, 107, 1034
- Spiegel E. A., Weiss N. O., 1980, *Nature*, 287, 616
- Stauffer J. R., Caillault J.-P., Gagne M., Prosser C. F., Hartmann L. W., 1994, *Astrophysical Journal Supplement Series* (ISSN 0067-0049), 91, 625
- Stern R. A., Schmitt J. H. M. M., Kahabka P. T., 1995, *Astrophysical Journal* v.448, 448, 683
- Sturrock P. A., 1999, *ApJ*, 521, 451
- Topka K., Golub L., Gorenstein P., Harnden F. R., Vaiana G. S., Avni Y., Rosner R., 1982, *ApJ*, 259, 677
- Vaiana G. S., Cassinelli J. P., Fabbiano G., Giacconi R., Golub L., Gorenstein P., Haisch B. M., Harnden F. R., Johnson H. M., Linsky J. L., Maxson C. W., Mewe R., Rosner R., Seward F., Topka K., Zwaan C., 1981, *ApJ*, 245, 163
- Voges W., Aschenbach B., Boller T., Bräuninger H., Briel U., Burkert W., Dennerl K., Englhauser J., Gruber R., Haberl F., Hartner G., Hasinger G., Kurster M., Pfeffermann E., Pietsch W., Predehl P., Rosso C., Schmitt J. H. M. M., Trümper J., Zimmermann H. U., 1999, *A&A*, 349, 389
- Voges W., Aschenbach B., Boller T., Brauninger H., Briel U., Burkert W., Dennerl K., Englhauser J., Gruber R., Haberl F., Hartner G., Hasinger G., Pfeffermann E., Pietsch W., Predehl P., Schmitt J., Trümper J., Zimmermann U., 2000, *VizieR On-line Data Catalog*, 9029, 0
- Zimmerman N., Oppenheimer B. R., Hinkley S., Brenner D., Parry I. R., Sivaramakrishnan A., Hillenbrand L., Beichman C., Crepp J. R., Vasisht G., Roberts L. C., Burruss R., King D. L., Soummer R., Dekany R., Shao M., Bouchez A., Roberts J. E., Hunt S., 2010, *ApJ*, 709, 733
- Zuckerman B., Song I., 2004, *Annual Review of Astronomy & Astrophysics*, 42, 685